Dynamics of vertical-cavity surface-emitting lasers in the short external cavity regime: Pulse packages and polarization mode competition

Andrzej Tabaka,[1] Michael Peil,[2] Marc Sciamanna,[3] Ingo Fischer,[1,2] Wolfgang Elsäßer,[2] Hugo Thienpont,[1] Irina Veretennicoff,[1] and Krassimir Panajotov[1,*]

[1]*Department of Applied Physics and Photonics (TW-TONA), Vrije Universiteit Brussel (VUB), B-1050 Brussels, Belgium*

[2]*Institute of Applied Physics, Darmstadt University of Technology, Schloßgartenstraße 7, 64289 Darmstadt, Germany*

[3]*Laboratoire Matériaux Optiques, Photonique et Systèmes (LMOPS), CNRS UMR-7132, Supélec, 2 Rue Edouard Belin, F-57070 Metz, France*

(Received 8 July 2005; revised manuscript received 26 September 2005; published 10 January 2006)

We study the influence of delayed optical feedback from a short external cavity (EC) on the emission dynamics of vertical-cavity surface-emitting semiconductor lasers (VCSELs). We find the emergence of pulse packages (PP) exhibiting characteristics which originate from the interplay of time-delay induced dynamics and polarization mode (PM) competition. We provide detailed analysis of the polarization dynamics applying complementary cross-correlation and spectral analysis techniques. The analysis reveals an interplay of the dynamics linked to the hierarchy of time scales present in the laser system: the fast time scale of the EC delay, the slower time scale of the PP, and the slow time scale of the polarization mode competition. For an analysis of the dynamics we provide a toolbox of methods adapted to the different relevant time scales and temporal variations of the dynamics. This complementary view unveils distinct changes in the relative oscillation phase of the two PM for increasing the injection current on both the fast and the slow time scales. Our results emphasize the significance of the polarization mode competition for PP dynamics in VCSELs, contrasting the observed behavior to what was reported for edge emitters.

DOI: 10.1103/PhysRevA.73.013810 PACS number(s): 42.65.Sf, 05.45.Jn, 42.55.Px

I. INTRODUCTION

To the best of our knowledge, the observation of the sensitivity of the emission properties of semiconductor lasers (SLs) to external optical feedback (OF) from a distant reflector has been reported already three decades ago [1]. Since then, the emission properties of SLs subject to OF have been intensively studied for different reasons. First, the high sensitivity of SLs to OF is very important from the application point of view. An unwanted reflection from optical components can easily destroy stable laser operation and induce complex emission dynamics [2–5]. Such instabilities can impair the functionality of various devices applying semiconductor laser technology, e.g., CD/DVD readout systems or optoelectronic telecommunication devices. On the positive side, sophisticated solutions have been developed utilizing delayed feedback for stabilization of the output of SLs and for narrowing the linewidth of the emitted light [6–9]. Furthermore, modern technology even aims for utilization of feedback-induced instabilities. Possible applications can be found in private communications [10–13], for optical data readout systems and frequency tuning [14], or chaotic LIDAR systems [15].

Second, SLs with OF are well controllable, nonlinear systems with delays. Therefore, such systems are well suited for an analysis of fundamental nonlinear dynamics phenomena of delay systems. The appearance of different dynamical regimes in such laser systems with delay is basically determined by the injection current and the main feedback parameters: the strength of the feedback, i.e., the amount of light that reenters the active region of the SL; the length of the external cavity (EC), and the feedback phase [16–18]. In the case of a long EC and moderate feedback, the stable emission of a laser is easily destabilized, leading to periodic, quasiperiodic, or chaotic regimes of the intensity dynamics. In the fully developed chaotic regime the linewidth broadens, evoking a degeneration of the coherence properties of the laser light. For that reason, this regime is referred to as "coherence collapse" (CC) [2]. An intriguing phenomenon belonging to this CC regime is the so-called "low-frequency fluctuations" (LFF), characterized by sudden, random dropouts of the laser intensity, followed by a stepwise recovery process [19,20]. A transition from these irregular dropouts to organized periodic states is observed when the EC is substantially shortened or when the injection current is lowered [21,22]. Indeed, for delay times of the order of the relaxation oscillation period or shorter, i.e., in the so-called short cavity regime, the regular pulse packages (PP) have been recently found in edge emitting semiconductor lasers (EELs) [18]. In this regime the dynamics of EELs sensitively depends on the feedback phase, comprising stable emission, periodic, quasiperiodic, and chaotic states. Typically, in this short EC regime, EELs emit pulses at the delay time modulated by a slower time-periodic envelope [18,23,24], forming pulse packages.

Recently, OF induced dynamics of vertical-cavity surface-emitting lasers (VCSELs) has attracted considerable interest. It has been demonstrated that VCSELs are similarly sensitive to external OF as EELs [25]. However, VCSELs differ from conventional EELs by their much shorter cavity length (usu-

*Also at Institute of Solid State Physics, 72 Tzarigradsko Chaussee Blvd., 1784 Sofia, (Bulgaria).

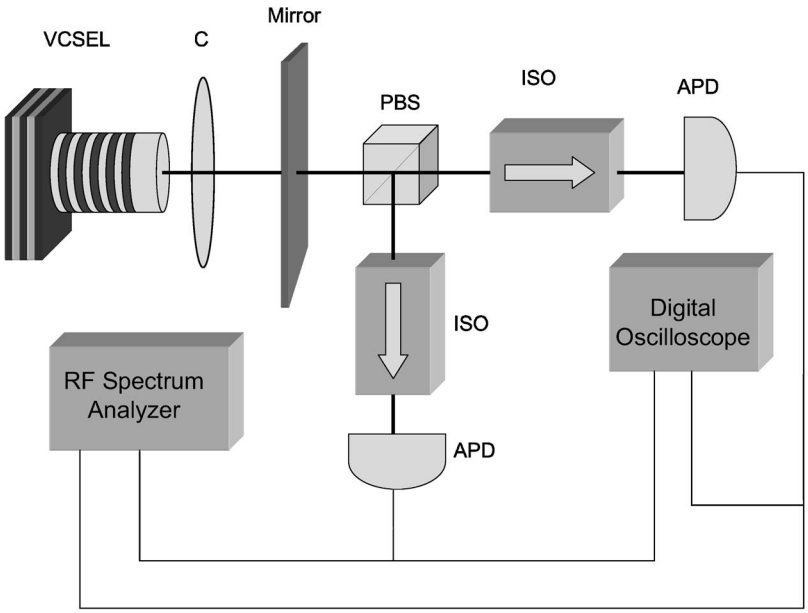

FIG. 1. Schematic illustration of the experimental setup: *C* is the collimating lens; PBS, polarizing beam splitter; ISO, optical isolators; APD, avalanche photodiodes.

ally of the order of λ) which restricts emission to one (single) longitudinal mode. VCSELs also emit circular output beams allowing for easier implementation into optical fiber communication systems and integrability in two-dimensional arrays. However, the circular geometry and the surface emission of VCSELs does not introduce strong anisotropies to fix the polarization of the emitted light. Nevertheless, VCSELs of small apertures typically emit light in one of the two orthogonally (*x* and *y*) linearly polarized directions. However, as the injection current increases, switching from one polarization mode (PM) to the other with orthogonal polarization direction can be observed [26–29]. These polarization instabilities become important in the case of OF as well. The existence of the two PMs in VCSELs can give rise to an additional polarization mode competition dynamics in the presence of feedback [30–32]. So far, research on OF induced dynamics of VCSELs has mainly focused on VCSELs with long ECs, while a detailed analysis of the dynamics of VCSELs with short ECs is still lacking.

In this manuscript we address this topic and present results of studies on the polarization resolved dynamics of VCSELs with OF in the short EC regime. In Sec. II we describe the experimental setup. In Sec. III we study the total intensity dynamics of the system and give experimental evidence for PP dynamics in VCSELs with short ECs. In Sec. IV we investigate the polarization resolved temporal dynamics in the PP regime and perform a detailed study of PM competition on fast and slow time scales of the dynamics. Detailed discussion of the experimental results is given in Sec. V. Final remarks are given in Sec. VI.

II. EXPERIMENTAL SETUP AND VCSEL CHARACTERISTICS

In this section, we describe the experimental setup which we use for the detailed characterization of the dynamics of a VCSEL with OF operating in the short EC regime. A scheme of the experimental setup is shown in Fig. 1. We use an etched air-post $Ga_xIn_{1-x}As$ VCSEL emitting at $\lambda = 968$ nm, whose temperature is stabilized to better than 0.01 °K (Profile TED 350). We control the injection current with an ultralow-noise current source (ILX LDX-3620) with a resolution of 0.01 mA and a stability of better than 1.0 μA. The wavelength emission of the VCSEL shifts with current by $d\lambda/dI = 0.35$ nm/mA and with the temperature by $d\lambda/dT = 0.05$ nm/K. The output beam of the VCSEL is collimated by an antireflection-coated aspheric lens (*C*) and directed towards a partially reflecting external mirror with a reflectivity of 30%. Thus, the mirror and the facet of the VCSEL form an external cavity. The phase of the feedback can be controlled by a piezoelectric transducer. We carefully align the feedback condition by adjusting the maximum threshold reduction. The polarizing beam splitter (PBS) splits the total intensity into its fundamental PMs, which are directed towards the two perpendicular detection arms. Each of the detection arms includes an optical isolator, in order to prevent any unwanted feedback from the detection branches towards the laser. We detect the light by means of two ultrafast photo detectors (APD) (New Focus NFI-1554-A-50) with 12 GHz bandwidth. The electronic signals from APDs are split into two branches and are further analyzed with a digital oscilloscope (Tektronix TDS7404) with 4 GHz bandwidth and sampling rate of 10 G samples/s, and an electrical spectrum analyzer (Tektronix 2755AP) with 18 GHz bandwidth. In order to observe the dynamics of the two polarizations simultaneously, the lengths of the two detecting branches have been matched carefully.

This experimental setup allows for a characterization of VCSEL and its dynamics. In Fig. 2, we plot the ratio P_x/P_y of the power in the two fundamental PMs as a function of the injection current, *J*. Without feedback, in Fig. 2(a)—in the so-called solitary laser case—the threshold current of the VCSEL is $J = 3.7$ mA and the VCSEL switches from the *y* to *x* polarization mode at a current of 4.2 mA. When OF is applied, the threshold is significantly reduced but the switching point remains almost unchanged in Fig. 2(b). Also the

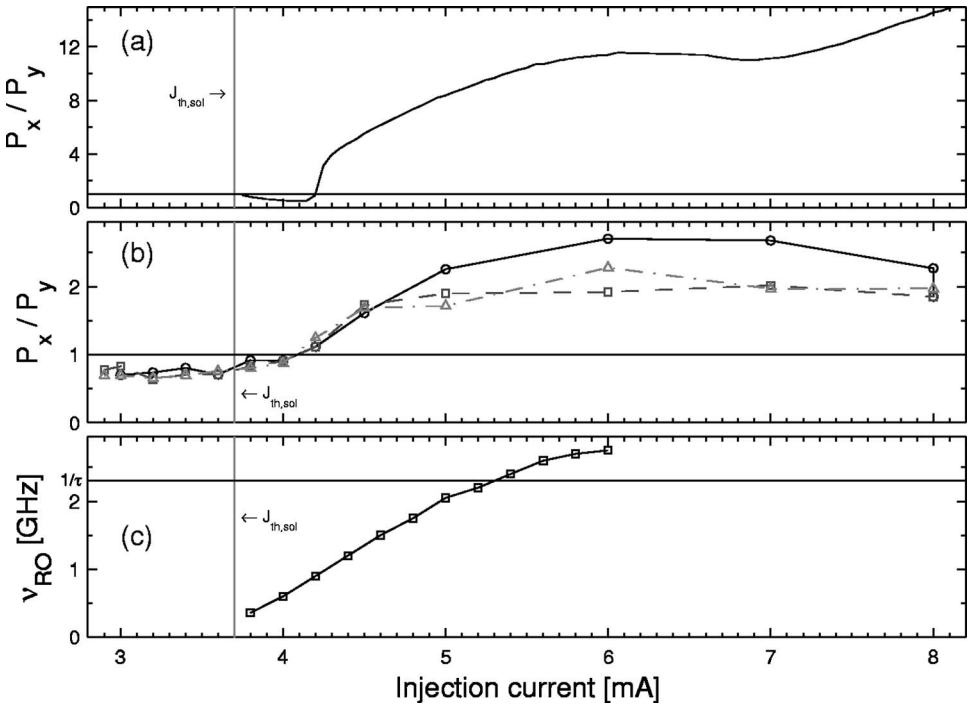

FIG. 2. In (a) and (b) we plot the ratio of the power emitted in the two PMs as a function of the injection current. Panel (a) represents the solitary case and (b) the case with feedback. Please note the different vertical scales. The three lines in panel (b) correspond to results for different EC lengths: solid line with circles, $L_{EC}=6.5$ cm; dashed line with squares, $L_{EC}=10.0$ cm; and dash-dotted line with triangles, $L_{EC}=16.0$ cm. The horizontal line of $P_x/P_y=1$ indicates the condition for which the power is equally distributed between the two polarization modes. In panel (c) we plot the relaxation oscillation frequency, obtained from a RIN analysis, as a function of the injection current. For $L_{EC}=6.5$ cm, the short EC condition is fulfilled for currents below $J=5.2$ mA.

PM suppression ratio is substantially decreased. This means that OF excites both PMs in the whole range of current operation. However, at low currents the y-PM dominates, whereas at high currents it is mostly the x-PM.

The RIN spectra allow us to analyze the dependency of the relaxation oscillations, ν_{RO}, in a function of J. At the EC length of $L_{EC}=6.5$ cm, the short cavity condition is fulfilled below $J=5.2$ mA, as illustrated in Fig. 2(c). In the following, we present a detailed analysis of the short EC dynamics of the VCSEL subject to OF for $L_{EC}=6.5$ cm.

III. PULSE PACKAGE DYNAMICS IN VCSELS

In the experiments, we adjust for $L_{EC}=6.5$ cm and concentrate on dynamics for currents below $J=5.2$ mA. For these conditions, the system fulfills the requirements for the operation in the short EC regime. In order to apply moderate feedback strength, we chose a mirror with a reflectivity of 30%, for which we measure a threshold reduction of about 22%. As presented in the following, for these conditions we are able to demonstrate PP dynamics in the total intensity of the VCSEL, and we are able to investigate properties of the PP dynamics in dependence on the injection current, J.

In Fig. 3, we present a set of time traces of the total intensity PP dynamics of the VCSEL together with the corresponding rf spectra at increasing values of J. In the time series, we observe bursts of laser intensity pulses at the delay time, similar to the ones shown in the case of RPP dynamics in EELs in the short EC regime [18]. The envelope of one sequence of pulses emitted at the delay time describes a package shape. For a regular sequence of pulses, the time between the drop-outs is referred to as PP period. In the corresponding rf spectrum, we observe peaks that reveal the presence of the two characteristic time scales, i.e., the peak at Ω_τ that is related to the inverse of the round-trip time in the external cavity (around 2.3 GHz) and the peak at the pulse package envelope frequency, Ω_{PP}, whose position moves by increasing the injection current J towards higher frequency ranges. We also mention a noticeable reduction of the regularity of the PP dynamics with J, which can be recognized by the broadening of the peak at Ω_{PP}, as well as by their decreased amplitude.

Complementary to the above time trace analysis and the corresponding rf spectra, we study the autocorrelation properties of the temporal behavior of the total intensity dynamics of the VCSEL in the PP regime. For the correlation analysis, positive values of the correlation function indicate correlated dynamics, while negative values reveal anticorrelated dynamics. If the correlation coefficient at a particular time lag is zero, one usually talks about noncorrelated behavior at this time lag.

For the same values of J as the ones in Fig. 3, we obtain the autocorrelation functions depicted in Fig. 4. In the autocorrelation functions, we find peaks at regularly spaced time intervals corresponding to the period of the envelope of the PPs. We notice a continuous decrease of PP period with J. On top of that, the insets in Fig. 4 also indicate the presence of the correlated pulses at the delay time (at around 0.4 ns) and multiples thereof. We mention that the pulses at the PP envelope, in the regime of low J, are present for long time intervals (more than hundred ns; i.e., several tens of pulse packages) revealing the characteristic regular feature of this dynamics. By increasing J, the amplitude of the peaks in the correlation function, corresponding to the PP envelope time scale, decreases and the correlation is kept for shorter and shorter time intervals [see Fig. 4(c)], similarly to the case of EELs [18]. Furthermore, we find less pronounced regularity of the fast pulsations, which becomes clear from the inset in Fig. 4(c). Finally, we come to the situation in Fig. 4(d), in which the PP envelopes are no longer distinguishable and the

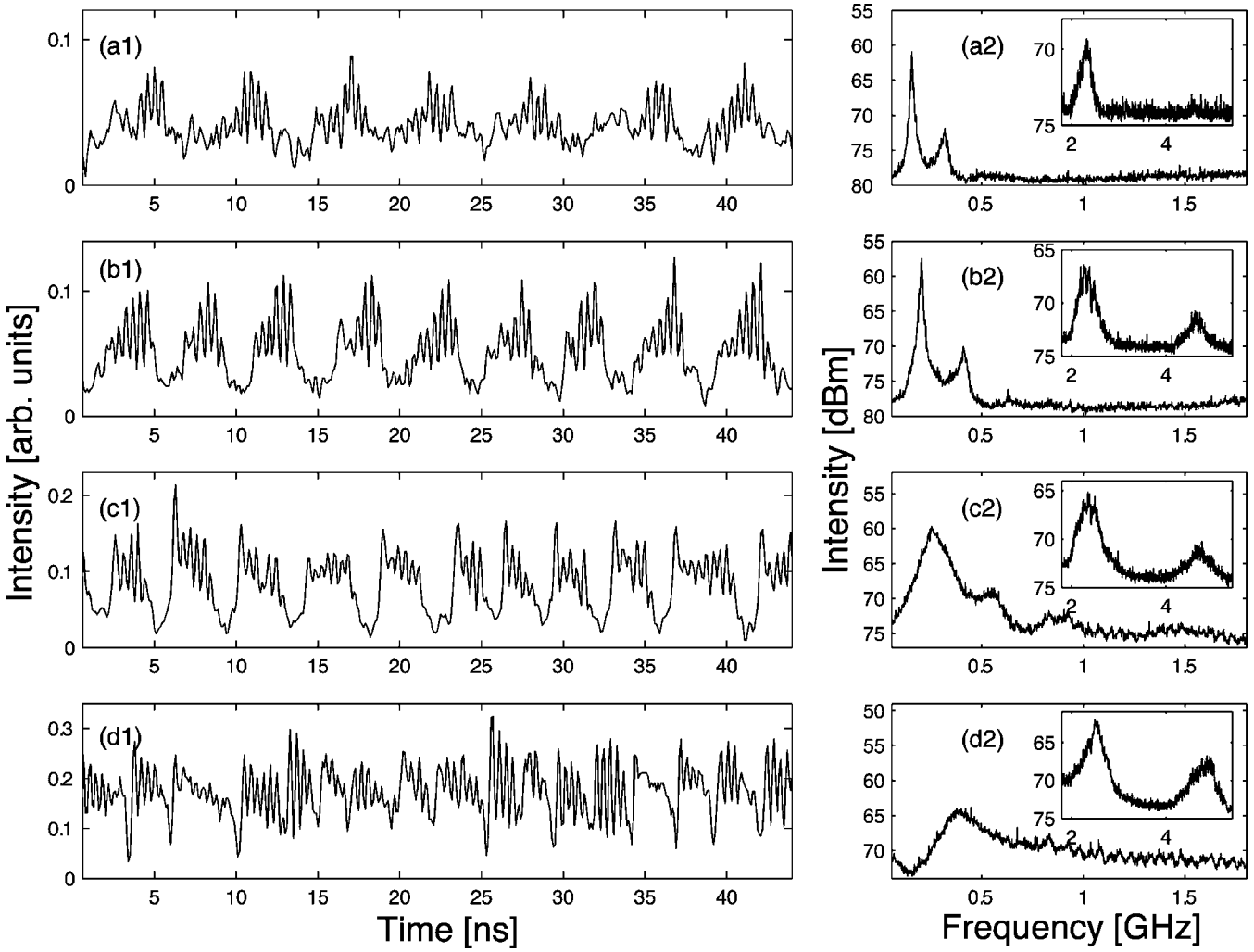

FIG. 3. In panels (1) we plot typical time traces of the total intensity emitted by the VCSEL in the PP regime, while we depict the corresponding rf spectra for increasing values of the injection current in panels (2). The EC length is 6.5 cm. In (a) $I=3.2$ mA, (b) $I=3.4$ mA, (c) $I=3.8$ mA, and (d) $I=5.0$ mA. Please note the different scales on the vertical axes.

correlation properties of the system are completely lost. Indeed, PPs still exist in Fig. 3(d1), but they are quite irregular leading to averaging out the corresponding autocorrelation peaks. Thus, the autocorrelation functions do not only confirm our previous observations of the characteristic features of the PP dynamics, but, even more, they provide further details about the change of the dynamical properties of the system as the injection current is varied.

In spite of many similar features of the regular pulse packages dynamics already observed in the case of EELs

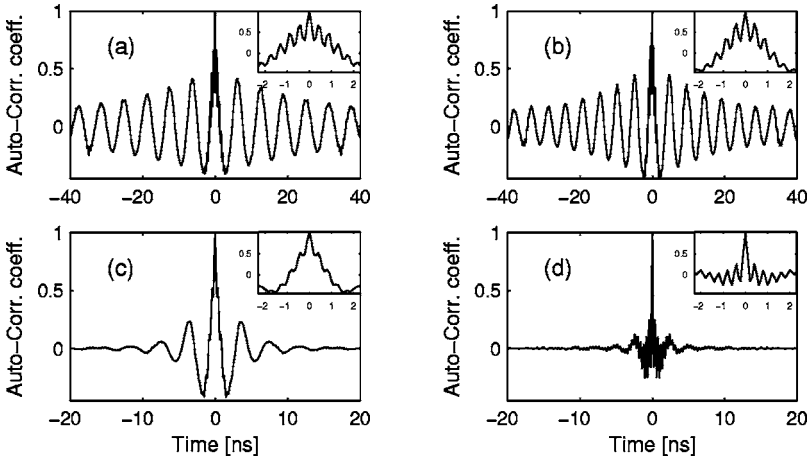

FIG. 4. The autocorrelation functions of the total intensity of VCSELs intensity time traces of Fig. 3 for the EC length of 6.5 cm. In (a) $I=3.2$ mA, (b) $I=3.4$ mA, (c) $I=3.8$ mA, and (d) $I=5.0$ mA.

[18,23,24] and the ones now presented in the case of VCSELs, we also find distinct differences. First of all, for the VCSEL we do not find qualitative changes in the intensity dynamics when changing the phase of the back-reflected light, as it is the case in EELs [23,24]. This is a striking difference as the phase sensitivity is a remarkable feature of the PP dynamics in EELs. In EELs, by changing the EC phase, one usually finds a characteristic cyclic scenario leading from stable laser operation to emission of pulse packages and back to stable state [23]. We notice that it was shown in [24], that in the case of EELs, as the delay time τ becomes larger than the relaxation oscillation period T_{RO}, the PP dynamics becomes less phase sensitive. For that reason, in the experiment we have verified the observation about the phase insensitivity in a range of external cavity lengths between 3–60 cm. We mention, that for the EC length of 6.5 cm the change of the wavelength λ with J of 0.35 nm/mA implies the variation of the phase over 2π corresponding to current intervals of around $\Delta J=0.02$ mA. Therefore, if there was a distinct phase sensitivity in the regime of the PP dynamics we would be able to recognize the appearance of different dynamics at different values of J with the used ultra-low-noise laser driver, although the resolution of the current source (of 1 μA) is insufficient to follow a cyclic scenario of the dynamics by changing the injection current, as it was the case in EELs in Ref. [23]. Another alternative for changing the phase is to keep the current and the temperature constant, while changing the EC length on a subwavelength scale. Even by doing so, in the case of the VCSEL, the qualitative phase insensitivity of PP dynamics proves to be independent of the EC length and variations of J. Thus, it is a distinct feature of VCSELs with OF in the short EC regime.

A first clue to the origin for this qualitative oscillation phase insensitivity is already given by a closer look at the dynamics, revealing that the amplitude and oscillation phase of the pulses emitted at the EC round-trip time in VCSELs significantly varies. We see that in the time traces, in Fig. 3, especially for higher values of current, some of the pulses seem to be emitted with less modulation depth. Sometimes the modulation is so small that they do not seem to be present at all. This results in a significant broadening of the peak at the delay in the corresponding rf spectra, when compared to the ones shown in the case of EELs [18]. This degraded regularity of the fast pulsations reveals a deterioration of the oscillation phase coherence of the dynamics preventing the emergence of more regular states, stable emission, periodic states, and regular PPs, which can be observed within the cyclic scenario in EELs.

Additionally, we find differences with respect to the PP dynamics in EELs in the change of the PP envelope shape with the injection current. The studies of regular PP dynamics in EELs indicate [33], that as J is progressively increased, one observes a gradual change in the shape of the PP envelope. At low values of J the laser fires pulses at the delay τ with continuously decreasing amplitudes. If J increases, the amplitude of the pulses emitted within one package first continuously increases and after reaching the maximum, progressively decreases. In VCSELs the situation seems to be reversed. At low values of J the amplitude of the pulses within one envelope first increases and then decreases. At higher levels of J the laser first emits pulses with high amplitudes while the amplitude of the following pulses progressively decreases. This change of the shape of the PP envelope in EELs has been identified in [33] as being due to the approach of another dynamical regime, which is characteristic for long external cavities, in which the laser emits not only pulses at τ but also exhibits secondary pulsations. The origins of these pulsations were related to the presence of the relaxation oscillations in semiconductor lasers. We mention that in our experiments with VCSELs, due to the limited bandwidth of the oscilloscope, we observe the presence of the secondary pulsations in the time traces only if the cavity is longer than 10 cm and the injection current is sufficiently high. However, these frequencies lie within the detection bandwidth of the rf spectrum analyzer, but we do not find evidence for corresponding relaxation oscillation dynamics in the rf spectra.

IV. POLARIZATION PROPERTIES OF PP DYNAMICS IN VCSELS

In the previous section, we have characterized the total intensity dynamics of the VCSEL, subject to external OF in the short cavity regime. We have demonstrated PP dynamics for VCSELs and compared the dynamics to typical PP dynamics of EELs. We have identified many similar features but also we have revealed characteristic differences. These differences give rise to questions about the origins of the interesting properties of the dynamics of VCSELs. Our results, obtained so far, suggest that the presence of the two linear polarization states might influence the PP dynamics and destroy the regularity in the system. We will address the question about the role of the interactions between the two PMs in VCSELs operating in the PP regime in this section.

A. Polarization resolved time traces

The polarization resolved PP dynamics is depicted in Fig. 5, for different values of the injection current. In black (gray) we plot the $x(y)$-PM of the VCSEL. At the lowest value of the injection current, $J=3.2$ mA, in Fig. 5(a), similarly as in the case of the total intensity dynamics [see Fig. 3(a1)], the amplitude of the peaks is still small and the shape of the single pulse package envelope is not very regular. However, the envelope of the packages can be clearly identified, which indicates that the PP in the two PMs are almost periodic with a characteristic frequency of Ω_{PP}. The PP dynamics in the two PMs can be much better recognized at $J=3.4$ mA, in Fig. 5(b). We notice that the polarization resolved PP dynamics is not as regular as for the total intensity, in Fig. 3(b1). The reason for this is that we observe PM competition, underlying the PP dynamics, reducing the regularity of the PP dynamics in each PM. This mechanism becomes more relevant at a higher injection current, approaching the polarization switching point. Accordingly, we find a gradual loss of the regularity in the PP dynamics as J is increased from 3.2 to 3.8 mA.

A closer look at the dynamics presented in Fig. 5 reveals that in some cases the PP dynamics temporarily takes place

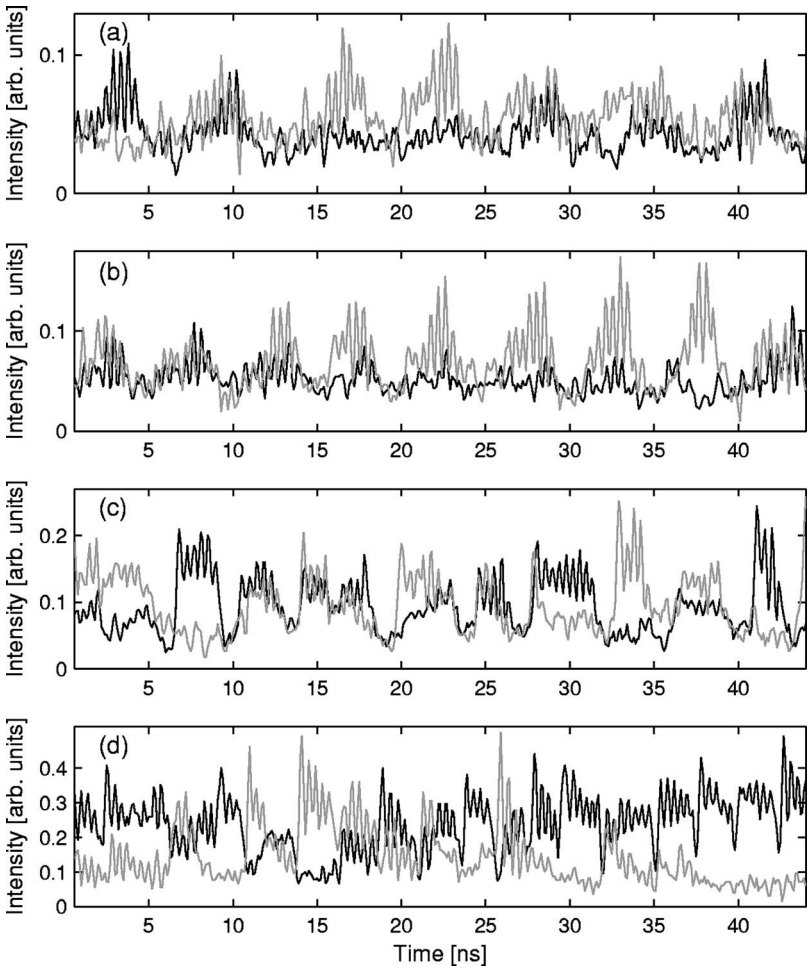

FIG. 5. Polarization resolved dynamics of a VCSEL in the PP regime at different values of the injection current. In black (gray) we plot the $x(y)$-PM of the VCSEL. The EC length is around 6.5 cm. In (a) $I=3.2$ mA, (b) $I=3.4$ mA, (c) $I=3.8$ mA, and (d) $I=5.0$ mA.

in one of the PMs only, while the second mode is almost turned off. In other cases the PP dynamics take place in the two PMs simultaneously. We refer to the first case of dynamics, in which the pulses are emitted in one PM only, as type I PPs. The second case of dynamics, in which the PP dynamics take place in the two PMs simultaneously, we call type II PPs. Similar interplay of the feedback induced complex dynamics and PM competition in VCSELs has been found numerically by Sciamanna *et al.* in [34] for LFF dynamics in the long EC regime and later experimentally confirmed by Sondermann *et al.* in [32] and Naumenko *et al.* in [35].

B. Cross-correlation analysis of pulse packages

In order to analyze the behavior of the polarization resolved dynamics qualitatively, we study the cross-correlation properties of the PMs during the PP dynamics. In Fig. 6, we plot the cross-correlation functions of the full time traces of the two PMs in the regime of PP dynamics at different values of the injection current. In this way, we are able to obtain information about the regularity of the system at different time scales and also we can extract the characteristic correlation time between the dynamics of the PMs.

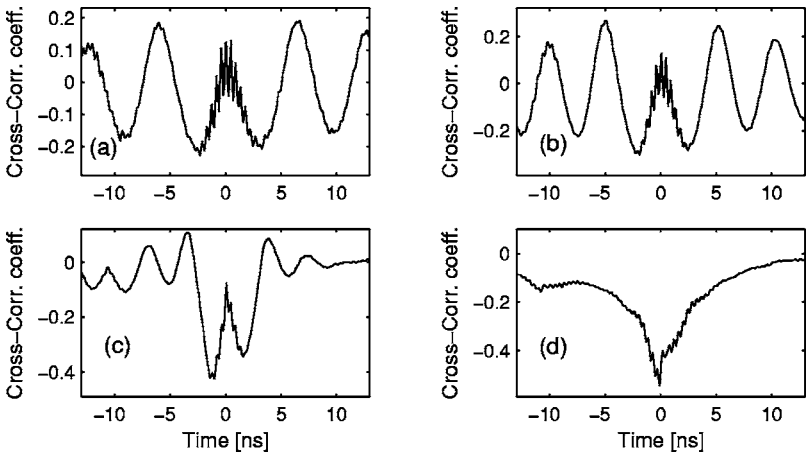

FIG. 6. Cross-correlation functions for the EC length of 6.5 cm. In (a) $I=3.2$ mA, (b) $I=3.4$ mA, (c) $I=3.8$ mA, and (d) $I=5.0$ mA.

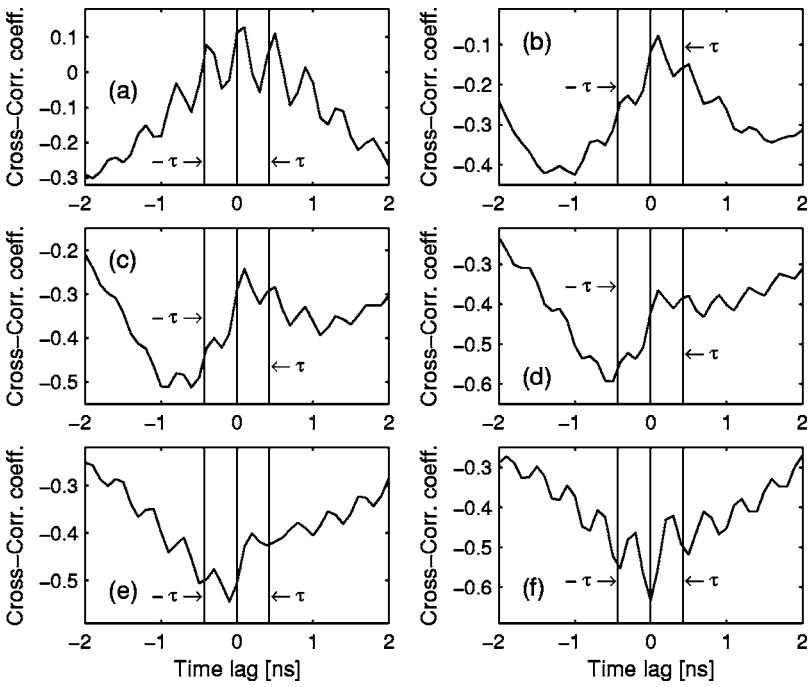

FIG. 7. Cross-correlation functions around zero time lag for EC length of 6.5 cm at different values of the injection current. In (a) $I=3.4$ mA, (b) $I=3.8$ mA, (c) $I=4.0$ mA. (d) $I=4.2$ mA, (e) $I=5.0$ mA, and (f) $I=6.0$ mA

At the lowest value of J, in Fig. 6(a), we observe regularly spaced maxima of the correlation function corresponding to the period of the PP envelope. By increasing the injection current, in Figs. 6(b)–6(d), we observe a continuous decrease of the modulation amplitude at the time scale of the multiples of the PP envelope until the peaks completely vanish, which we demonstrate in Fig. 6(d). First, this shows that the regularity of the PP dynamics is progressively lost and, second, that the dynamics dominantly persists for longer and longer time intervals in one PM. Moreover, in the regime of high injection currents, well above the polarization switching point, the cross-correlation function becomes negative for all time lags. This substantial change of the shape of the cross-correlation function can be associated with a remarkable change of the PP dynamics reflecting a gradual transition from type II PP to type I PP. Indeed, the results, presented in Fig. 6, confirm that in the low range of current the dynamics is mostly type II PP, whereas well above the solitary threshold it progressively becomes type I PP, although the PM suppression ratio P_x/P_y is still comparatively small, according to Fig. 2(b).

Additionally, in Fig. 6, we find correlation peaks reflecting the correlation properties of the pulses emitted at each round-trip time. In order to better reveal the correlation properties of the PP dynamics at this short time scale, we replot in Fig. 7 the cross-correlation functions for different injection currents, focusing on the vicinity of zero time lag and few multiples of the delay.

In Fig. 7(a), we clearly see the correlated peaks at the delay and multiples thereof. On top of that, superimposed on the delay time spaced peaks, we find a positive correlation at zero time lag revealing not only that in most cases the PPs are observed in the two PMs simultaneously, but also that the PP dynamics of the two modes within one package is correlated, i.e., the pulses are fired mostly at the same moment of time. By increasing the injection current, we find in Figs. 7(a)–7(f) that the cross-correlation coefficients at zero time lag and the delay continuously decrease in a similar way as the pulses at the PP envelope. It means that the dynamics becomes more and more anticorrelated at this time scales. And in a similar way as in the PP envelope case, this continuous decrease is also related to the transition from type II PP to type I PP as we change the injection current.

However, in Fig. 7, we find even more information about the intriguing particularities of the mode competition dynamics in VCSEL subject to feedback in short cavity regime. In Fig. 7(a), we observe a clear maximum of the cross-correlation function around zero time lag and also we see positive peaks at the delay time (and multiples thereof), which means that the emission of peaks takes place in a correlated manner at low pumps. As we increase the injection current, we do not find the maxima of the correlation function precisely at zero time lag and at the delay, but these peaks are rather shifted to the right. Due to limited resolution of the oscilloscope (0.1 ns), this shift is best observed in cases 7(d)–7(f). As we increase the current, on average, the emission of pulses in one PM is delayed with respect to the other PM. This average delay slightly increases with the current, and leads to fully anticorrelated behavior of the pulse emission at very high currents, see Fig. 7(f).

We note that the cross-correlation functions are not symmetric around zero except for the ones depicted in cases (a) and (f), in Fig. 7. In the nearly symmetric cases, in (a) and (f) in Fig. 7, the dynamics keeps the correlation properties during the whole duration of the PP envelope. In Fig. 7(a), we find that the PP dynamics in the two PM appears in the same moments of time and it is on average correlated during the time of the PP envelope, whereas, in Fig. 7(f), the PP dynamics appears consecutively in the two PM. If the cross-correlation function is not symmetric, as it is depicted in cases 7(b)–7(e), the average correlation of the PP dynamics changes within a single pulse package envelope. It also

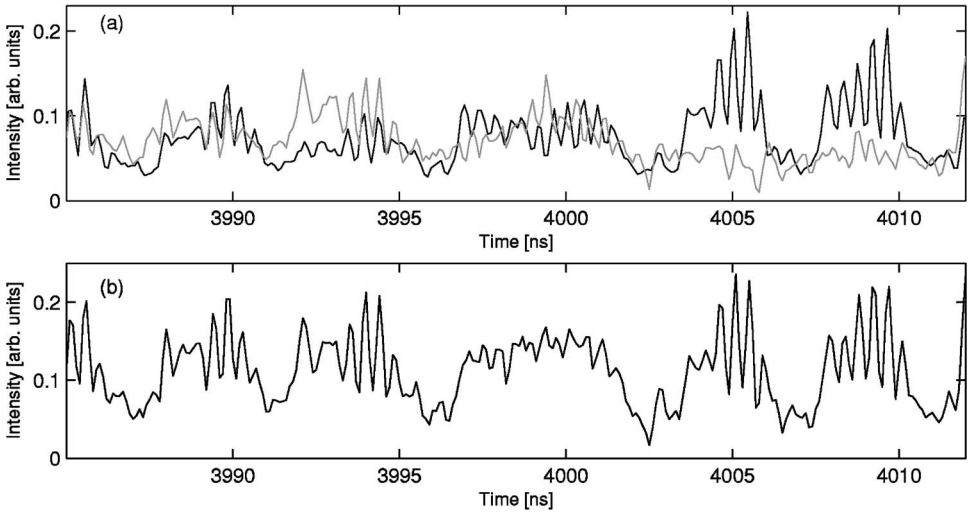

FIG. 8. In (a) polarization resolved time traces in PP regime and in (b) the sum of the two PMs, illustrating continuous change of the amplitude of the peaks. The parameters are $L_{EC}=6.5$ cm and $J=3.6$ mA.

means that the PP dynamics may not always persist in one of the PM until the end of the PP envelope. Moreover, the lower cross-correlation coefficient on the left-hand side, in Figs. 7(b)–7(e) shows that the *x*-PM is strongly anticorrelated with the pulses that are emitted before the appearance of the present pulse and less anticorrelated with the pulses that are emitted after the appearance of the present pulse in the *y*-PM. Therefore, the two PMs are strongly coupled in the PP regime, and the appearance of PP dynamics in one PM triggers the emission of pulses in the other PM.

As we have discussed above, the effect that contributes to the negative correlation at zero time lag, as it is the case in Fig. 7(f), is mainly related to the fast dynamics on the time scale of a single round trip. In order to clarify the emergence of this negative correlation property, we compare an enlarged segment of the polarization resolved time traces with the sum of the two time series of the PMs of the VCSEL. The corresponding time series are depicted in Fig. 8. In the sum of the two PM intensities, illustrated in Fig. 8(b), we find that the regularity of the PPs is not destroyed by the PM competition. In addition to this, the sum of the two PM intensities reveals that PM competition is a relevant mechanism explaining the changes of the amplitude of the fast pulsations on the time scale of the delay time for the total intensity dynamics, discussed in the previous section. A closer look at the time series at the time interval around 4000 ns, in Fig. 8(b), uncovers a significant decrease of the amplitude of the peaks at the delay time. At this time, the corresponding polarization resolved traces, in Fig. 8(a), are anticorrelated. On the contrary, the pulses at the time interval around 3990 ns, in Fig. 8(a), are correlated, resulting in large amplitude peaks in the sum of the traces, in Fig. 8(b). Therefore, we can associate the variation of the amplitude of the pulses in the total intensity, in Fig. 3, with the polarization dynamics taking place during one PP. We notice that similar analyses of the correlation behavior and its variability were already reported in Ref. [35]. Despite these changes of correlation among the two PMs at comparable intensities, we find a tendency that the momentary difference of the power of the PM influences the correlation of the pulses emitted in the two PMs.

We illustrate this tendency via the time series depicted in Fig. 9, in which we present the polarization resolved time series as solid lines, recorded with a bandwidth of 4 GHz, together with the same but low-pass filtered time series, with the cut-off frequency of the filter being 100 MHz, depicted as dotted lines. In Fig. 9, the intensity dynamics of the *x*-PM is represented in black, while that of the *y*-PM is shown in gray. We have selected an injection current of 4.5 mA, which is close to the polarization switching point. In this way, we are able to compare the correlation properties of the fast pulses, i.e., the positions and the amplitudes of the peaks, in relation to the momentary mean intensity of the modes.

As illustrated in Fig. 9, for large differences of the PM intensities, the pulses tend to be anticorrelated, while we find correlation predominantly for time intervals with equal intensities of the two PMs. For a current value of $J=4.5$ mA, close to the polarization switch, we have a frequent change of the dominant PM and, therefore, a frequent and gradual change between correlation and anticorrelation of the pulses. This is a result of a permanent interplay between the PM competition and feedback induced dynamics. In contrast, we find anticorrelation of the fast pulses of the PMs for injection

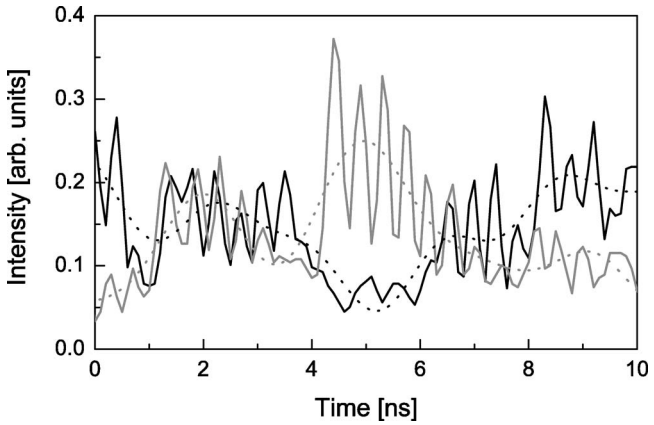

FIG. 9. Polarization resolved time traces recorded with 4 GHz (solid lines) and same time traces filtered with a 100 MHz low-pass filter (dotted lines). A comparison reveals the dependence of the short-time correlation properties of the fast pulsations on the momentary intensity difference of the polarization modes. The *x*-polarization mode is represented in black and the *y*-polarization mode in gray. The parameters are $L_{EC}=6.5$ cm and $J=4.5$ mA.

currents well above the polarization switching point, contributing to the negative cross-correlation coefficients at zero time lag and multiples of the delay as it is evident, in Figs. 6(d) and 7(f). The reason for this anticorrelation can be found in the domination of the x-polarization mode and the higher power available for the pulses, underlying the relevance of PM competition on this time scale of the dynamics.

C. Spectral analysis

In this section, we complement the analysis of the PM dynamics presented above, by exploring the correlation properties of the two PMs of the VCSEL by analyzing the spectral properties of the dynamics. The applied method allows for the investigation of the phase coherence of the two PMs in the dynamical system and has been successfully used in the case of multimode EELs [36,37]. Our goal is to extract the correlation properties of the dynamics for different characteristic frequencies involved in the dynamics. To this end, we compare the power spectral density (PSD) of the total intensity with the PSDs of the two PMs. We use the following notation: $P_x(\Omega), P_y(\Omega)$ represent the value of the PSD at a particular frequency Ω of the dynamics of the x-(y-) PM, measured from the rf spectra, and $P_{tot}(\Omega)$ represents the measured PSD of the total intensity dynamics of the VCSEL. We introduce the incoherent sum $S_{inc}(\Omega)=P_x(\Omega)+P_y(\Omega)$, and the in-phase sum $S_{ph}(\Omega)=[\sqrt{P_x(\Omega)}+\sqrt{P_y(\Omega)}]^2$ of the measured PSDs of the two PMs at a particular frequency Ω. Therefore, the oscillation phase coherence of the intensity dynamics in the case of the two PMs of VCSEL can be classified as follows [36,37]. For perfectly in-phased dynamics we have $P_{tot}(\Omega)=S_{ph}(\Omega)$ and for perfectly antiphase dynamics we have $P_{tot}(\Omega)=0$. For all intermediate states the following condition is fulfilled: $0<P_{tot}(\Omega)<S_{ph}(\Omega)$. For the latter, we distinguish between predominantly in-phase states: $P_{tot}(\Omega)>S_{inc}(\Omega)$; and predominantly antiphase states: $P_{tot}(\Omega)<S_{inc}(\Omega)$.

In Fig. 10, we depict the measured PSD of the total intensity P_{tot} together with the incoherent sum S_{inc} and the in-phase sum S_{ph} of polarization resolved PSDs as a function of the injection current. In each plot, we observe peaks corresponding to the PP envelope frequency Ω_{PP} and peaks at the delay Ω_τ (and multiples thereof). For each value of J, we observe anticorrelated dynamics in the low frequency range $\Omega_{LF}<\Omega_{PP}$, i.e., $S_{inc}(0)\gg P_{tot}(0)\approx 0$. This feature reflects the presence of the slow mode hopping dynamics between the two polarization states, characteristic for PM competition, in the whole range of currents. In other words, the PP dynamics is superimposed on the low-frequency mode hopping dynamics. This means that although the PP dynamics might persist in two PMs simultaneously, there is a continuous change of the amplitude of the PPs in each PM, induced by PM competition.

At the lowest value of the injection current $J=3.2$ mA, we see that at Ω_{PP}, $P_{tot}(\Omega_{PP})$ is almost at the level of $S_{ph}(\Omega_{PP})$, which indicates that the dynamics is in phase. As can be seen in Figs. 10(a)–10(d), this in-phase dynamics at (Ω_{PP}) is progressively lost for increasing J and gradually changes to antiphase dynamics for currents well above the polarization switching point. This result confirms our previous findings, obtained from the cross-correlation analysis presented in Sec. IV B, in which the pulse packages in the two PMs are mainly correlated for low current levels, while they are predominantly anticorrelated for high current levels.

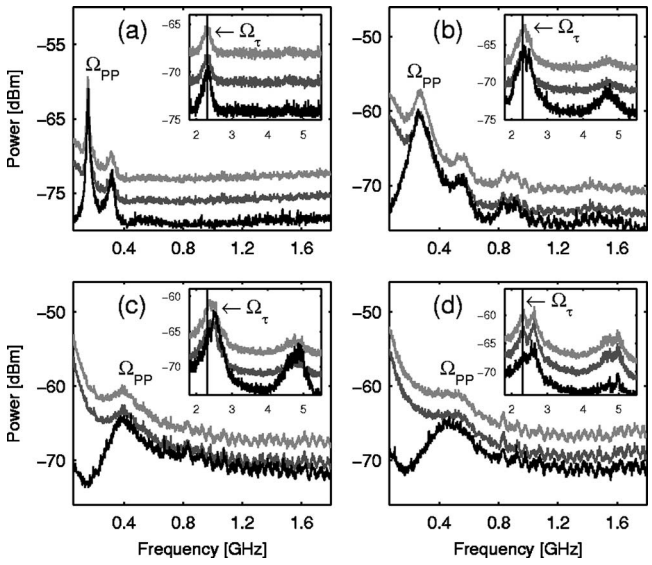

FIG. 10. Comparison of the measured PSD of the total intensity P_{tot} (in black), the incoherent sum S_{inc} (dark gray), and the in-phase sum S_{ph} (light gray) of polarization resolved PSDs at different values of the injection current. In (a) $J=3.2$ mA, (b) $J=3.8$ mA, (c) $J=5.0$ mA, and (d) $J=6.0$ mA. The length of the cavity is $L_{EC}=6.5$ cm. The vertical lines in the insets represent the inverse of the delay. Please note the different vertical scales.

In the following, we focus on the high-frequency part of the dynamics comprising the fast pulsations at the round-trip frequency. The corresponding frequency range is depicted in the insets of Fig. 10. In the inset of Fig. 10(a), we see that $P_{tot}(\Omega_\tau)\leqslant S_{inc}(\Omega_\tau)$. This shows that the dynamics of the PMs at Ω_τ is either incoherent (no fixed phase relation of the dynamics of the PMs at Ω_τ sustains) or slightly antiphase, on the long time average. For $J=3.8$ mA, in Fig. 10(b), approaching the polarization switching point, P_{tot} is on the same level as S_{inc} at the frequency Ω_τ. Indeed, for the later two cases it is difficult to distinguish between incoherent and antiphase dynamics. Time resolved correlation methods will be applied later on to clarify this issue.

A further increase of J exposes an interesting feature. The measured PSDs of the two PMs in Fig. 10(d) reveal a two-peak structure in the vicinity of Ω_τ. The peak on the left side is close to the inverse of the EC round-trip time, while the position of the peak on the right side shifts with J. Interestingly, the double-peaked PSD reveals different correlation behavior for each of the two peaks. The peak on the left side shows antiphase dynamics, while the one on the right side exhibits in-phase dynamics. An explanation of the origin of this double-peak structure is beyond the scope of this paper, but we remark that a similar double-peaked structure at Ω_τ is commonly known [30,35] in the case of the long cavity regime of LFF dynamics. Recently, the emergence of this double-peak structure has been related to an interplay be-

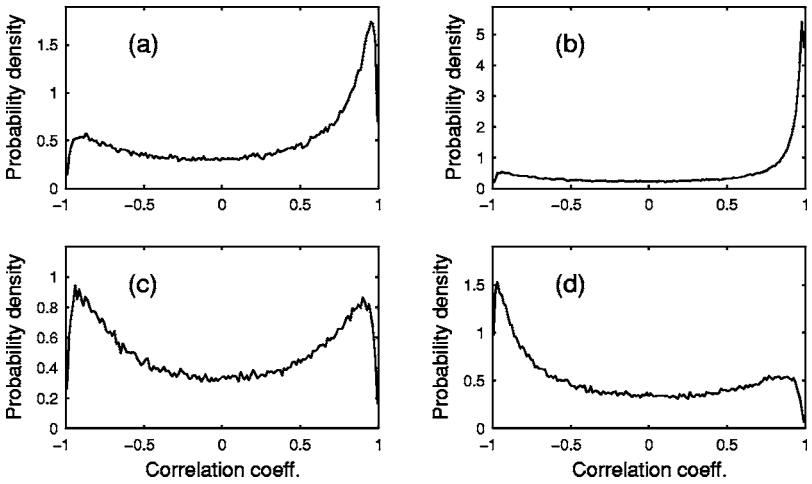

FIG. 11. Low-pass filtered probability density vs cross-correlation coefficient at zero lag at different values of the injection current. In (a) $J=3.2$ mA, (b) $J=3.8$ mA, (c) $J=4.5$ mA, and (d) $J=6.0$ mA. The histogram is normalized such, that integral over probability distribution is 1. The length of the cavity is $L_{EC}=6.5$ cm.

tween the external cavity round-trip frequency and the relaxation oscillation frequency [38].

Here, again, we focus on the influence of an increased injection level on the correlation properties of the fast intensity pulsations of the VCSEL which are related to the delay term. For increasing J, we find successively pronounced antiphase dynamics at Ω_τ. Our results show that the higher the injection current, the better the antiphase PP dynamics persists. This becomes clear from Figs. 10(c) and 10(d). This result also agrees with our previous result, obtained from the cross-correlation analysis and discussed in Sec. IV B, and demonstrates that the fast pulsations of the PMs tend to be anticorrelated for currents well above the polarization switching point.

Utilizations of the cross correlation and the spectral analysis for characterization of the PP dynamics of the two PMs of the VCSEL have verified the role of PM mode competition for the emergence of the total intensity dynamics. We have been able to analyze this effect on the relevant time scales of the PP dynamics. However, the above cross correlation and spectral analysis provide information on the time average properties of the system only, i.e., comprising temporarily different correlation states of dynamics. Therefore, in order to reveal the momentary cross-correlation properties, and to quantify the amount of correlated and anticorrelated dynamics that are taking place on the relevant time scales in the system, i.e., the time scale of the PP envelope, and the time scale of the delay, we complement our results by a time resolved correlation technique, which we will introduce in the following sections.

D. Low-frequency components of the PP dynamics

In this section, we analyze the temporal evolution of the correlation properties of the dynamics of the two PMs of the VCSEL. First, we focus on the temporal evolution of the correlation properties on the PP envelope time scale. To this end, we perform a sliding segment cross-correlation analysis on the low-pass filtered polarization resolved time traces of the laser intensity. This technique allows us to capture the time resolved correlation properties of the system. Of particular interest is the information about the influence of the mode competition on the dynamics on the time scale of a single pulse package. With the low-pass filtering of the time traces we remove the contribution of the fast dynamics on the time scale of the delay; the remaining dynamics are on the time scales longer than the period of the PP envelope. To this end, we average the measured time traces over a time window of twice the EC round-trip time. Then, we calculate the correlation coefficient of the low-pass filtered data for a segment of the time traces corresponding to the inverse of the cut-off frequency of the low-pass filter. After that, we repeat this procedure for the next interval, consecutively sliding the window along the time series. In this way, we obtain a set of cross-correlation coefficients in the range $[-1,1]$, reflecting the temporal evolution of the correlation properties with a resolution of the time scale of the PP envelope. We analyze the statistics of these coefficients and plot the results in the form of a histogram, which describes the probability density of the cross-correlation coefficient.

In Fig. 11, we present the histograms of the cross-correlation coefficient at zero lag of the low-pass filtered time traces of the two polarizations at different values of the injection current. At $J=3.2$ mA, in Fig. 11(a), we observe one clear maximum of the probability density function (PDF) close to a correlation coefficient of +1. This means that the two PMs are strongly correlated and the PP occur simultaneously in the two PMs, i.e., the PP dynamics of type II dominates at this level of the injection current. For an increase of the injection current to ($J=3.8$ mA), we even find a higher probability of type II PP dynamics, which is illustrated in Fig. 11(b). We note that in Fig. 6 this increase of the number of correlated events has led to an increase of the cross-correlation coefficient at the PP envelope time scale. However, this increase has not been captured by the spectral analysis in Fig. 10. This discrepancy might be due to insufficient sensitivity of the sampling oscilloscope in our experiment.

When increasing the injection current, we find a continuous transition from correlation to anticorrelation of the dynamics of the PMs. The transition takes place for intermediate values of $J\approx 4.5$ mA, where we find a situation, in which the statistics exhibit equal probability density for correlation and anticorrelation of the dynamics, which is presented in Fig. 11(c). This is the point with intermediate value of the

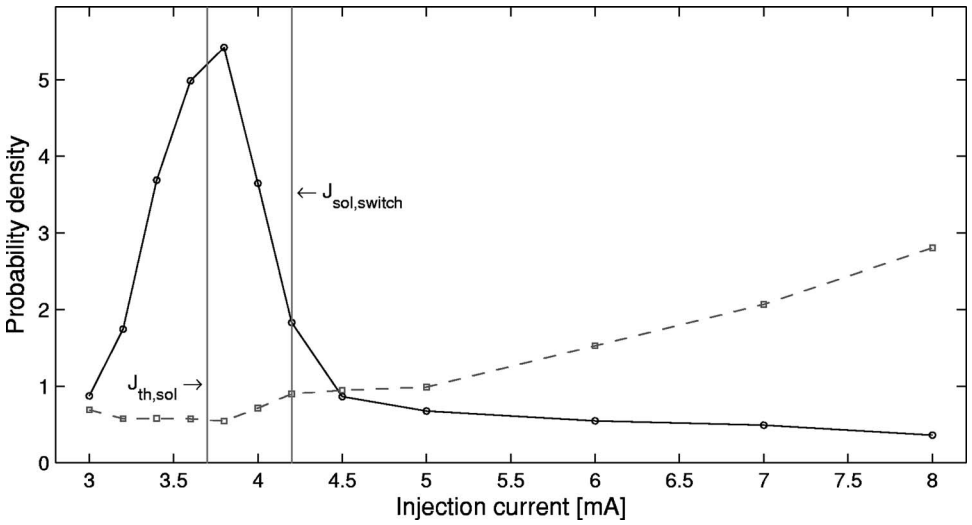

FIG. 12. Probability density as a function of the injection current. The solid line with points represents the peak probability density for correlation and the dashed line with squares represents the peak probability density for anticorrelation of the PP dynamics on time scale of a PP envelope. The type I PP dynamics overtakes the type II PP dynamics at J close to the solitary VCSEL polarization switching point.

polarization mode suppression ratio, presented in Fig. 2(b). Well above the polarization switching point, in Fig. 11(d), the dynamics are predominantly anticorrelated but there are still reminiscence of the correlated dynamics not revealed either by the average cross-correlated analysis, in Sec. IV B, or by the spectral analysis, in Sec. IV C.

We summarize our observations about the correlation properties on the slow time scales of the PP dynamics in Fig. 12, in which we plot the maxima of the PDF, like the ones presented in Fig. 11, representing the correlation and the anticorrelation of the dynamics, as a function of J. We find that for low levels of J, up to the approximate value of the solitary laser polarization switch, the PP dynamics of type II dominates. The probability for correlated dynamics continuously increases, reaching the maximum in the vicinity of the solitary laser threshold $J_{th,sol}$. We mention that this maximum can shift slightly depending on the cut-off frequency of the low-pass filter and the length of the sliding correlation window. Further increase of J leads to a continuous decrease of the probability density for correlated dynamics, while the probability density for anticorrelated dynamics continuously increases, equalizing the probability density for correlation close to the polarization switching point. This means that the dynamics of the VCSEL exhibits a transition from type II PP dynamics to type I PP dynamics. Intuitively, these results motivate an analogous analysis of the dynamics of the VCSEL feedback system on the time scale of the delay time, the second characteristic time scale.

E. High-frequency components of the PP dynamics

In this section, we adapt the time resolved cross-correlation analysis in order to get insight into the correlation properties of the high-frequency components of the PP dynamics, i.e., the dynamics on the time scale of the delay. The cross-correlation coefficients are calculated directly from the (unfiltered) measured data for a window length of twice the delay time, sliding the window consecutively along the time series. Then, we calculate the PDFs of the cross-correlation coefficients of the two polarizations at zero time lag and for different values of the injection current.

The results are presented in Fig. 13. The figure shows

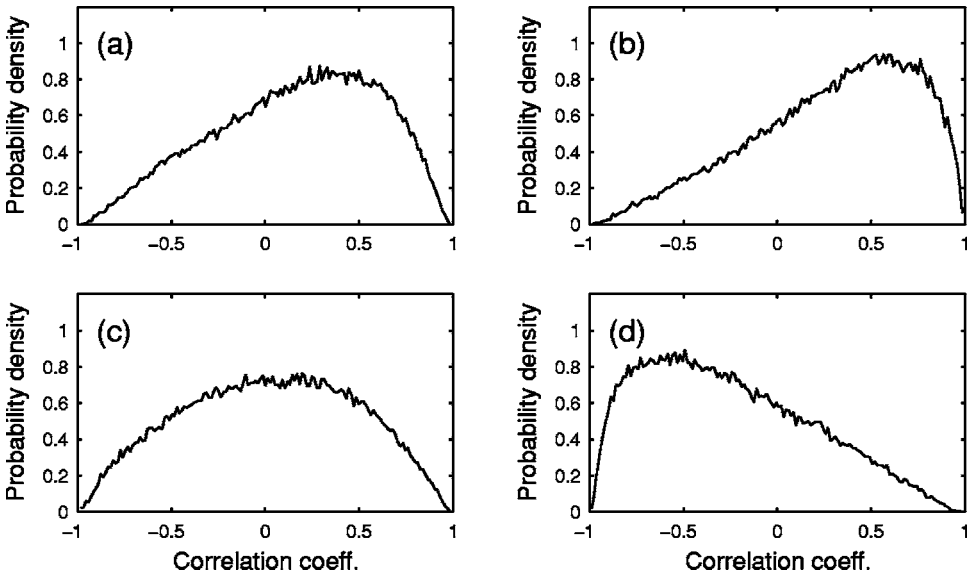

FIG. 13. Probability density vs cross-correlation coefficient at zero lag at different values of the injection current. In (a) $J=3.2$ mA, (b) $J=3.8$ mA, (c) $J=4.5$ mA, and (d) $J=6.0$ mA. The histogram is normalized such that the integral over probability distribution is 1. The length of the cavity is $L_{EC}=6.5$ cm.

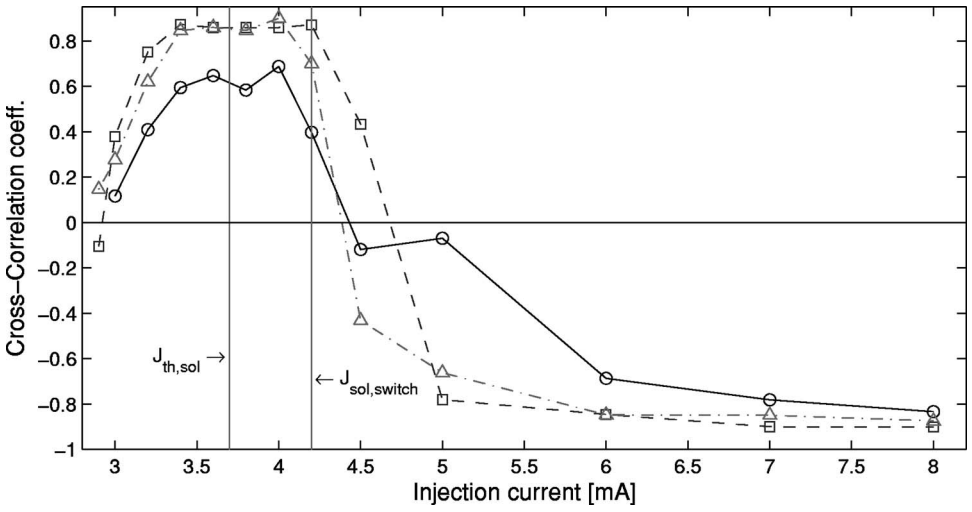

FIG. 14. Cross-correlation coefficient at zero lag in function of the injection current. Solid line with circles corresponds to the EC length of $L_{EC}=6.5$ cm; dashed line with squares corresponds to $L_{EC}=10.0$ cm; and dash-dotted line with triangles corresponds to $L_{EC}=16.0$ cm.

broad distributions of the cross-correlation coefficients with well-defined maxima at coefficients substantially deviating from −1 or +1, contrasting these histograms to that obtained for the low-pass filtered data presented in Fig. 11. Here, in Fig. 13, we see that the maxima of the PDFs shift with the change of J. At $J=3.2$ mA, in Fig. 13(a), we observe a clear maximum for positive cross-correlation coefficients which indicates that the dynamics is dominantly correlated on the time scale of the round-trip time. The maximum of the PDF for $J=3.8$ mA, depicted in Fig. 13(b), reveals an even higher correlation for pump currents close to the solitary laser threshold current. This increase of the correlation again might be connected with insufficient sensitivity of the oscilloscope at such a low value of J. Increasing further the injection current, we find that the maximum of the PDFs continuously shifts towards negative correlation coefficients. Eventually, at very high currents, the fast pulses emitted in the two PMs are dominantly anticorrelated, which becomes clear from Fig. 13(d) illustrating the behavior for $J=6.0$ mA.

An interesting consequence of this transition between the two states, in which the pulses emitted in the two PMs at the delay are either dominantly correlated or dominantly anticorrelated, is the intermediate state in which the maximum of PDF is located around zero. At first sight, one might interpret this situation as an indication for uncorrelated dynamics. However, the cross-correlation analysis presented in Fig. 7 and detailed analysis of the corresponding time traces reveals that the broad distribution of the cross-correlation coefficients originates from strong PM competition on this time scale, permanently changing the phase relation between the pulses of the PM as indicated in Fig. 9. This is due to the fact that the phase relation depends on the momentary difference of the modal intensities, as presented in Fig. 9. On average, this strong PM competition leads to a successive phase shift between the two PMs. As we have suggested, in Sec. IV A, the appearance of a pulse in one PM triggers the appearance of a similar pulse in the orthogonal PM. As the correlation properties of the pulses frequently change, it leads to the broad probability distribution functions, as presented in Fig. 13.

We summarize our observations about the high-frequency components of the PP dynamics in VCSELs, in Fig. 14, by plotting the maximum of the PDF depicted in Fig. 13, as a function of injection current. Our results show that in low ranges of J, the maximum of the cross-correlation coefficient increases with J. This indicates that the pulses emitted in the two PMs become more and more correlated. Interestingly, the cross-correlation function takes a maximum close to the solitary laser threshold, $J_{th,sol}$. After passing the maximum, at higher injection currents the cross-correlation coefficient continuously decreases. This shows that the fast pulses in the two PMs become more and more anticorrelated. The system switches its correlation properties from positive to negative correlation in the vicinity of the solitary VCSEL polarization switching point, $J_{sol,switch}$, which coincides with the switching point of VCSEL subject to feedback.

V. DISCUSSION

The continuous shift of the maximum of the PDFs with the injection current indicates that two mechanisms are mainly involved in the emergence of the PP dynamics of VCSELs in the short EC regime. These are the delay-induced instabilities, on the one hand, and the PM competition, on the other hand. A comparison of Fig. 14 with Fig. 2(b) shows that the cross-correlation coefficient is mainly positive at the ratios of the PM intensities around 1, and for small current values, below the polarization switching point. Furthermore, in Fig. 14 we find maximal cross-correlation coefficients for currents close to the solitary laser threshold. We note that this result might be connected with low sensitivity of our sampling oscilloscope as this maximum is not found in the spectral analysis, in Fig. 10. In this low current regime, type II PP dynamics dominates, i.e., the dynamics simultaneously appears in the two PMs, see Fig. 12. This situation changes, however, for higher injection currents, where one PM dominates during the PP dynamics. In this high current regime the pulses at the delay are mostly fired in an anticorrelated manner.

As we have illustrated in Fig. 7, the progressive change of the dynamics is connected also with a phase shift between the emission of pulses in the two PMs, from 0 at low currents to π at high currents. Near the polarization switching point, the role of the dominant mode changes frequently, as shown in Fig. 9, but there is an average phase shift of $\pi/2$ between the emission of pulses in the two PMs, illustrated in Fig. 7. Therefore, the maximum of the PDF, in Fig. 13, exhibits a broad distribution of the cross-correlation distribution around zero.

Moreover, the nonsymmetric distribution of the cross-correlation functions around zero time lag, in Fig. 7, shows that the appearance of the dynamics in one PM can trigger the emission of pulses in the other PM. Considering the fact that neither of the two PMs is the dominant mode in the regime of low current, the feedback can induce the PP dynamics in the two PMs simultaneously. Indeed, mostly type II PP is observed, as illustrated in Fig. 12. Our observations indicate, therefore, that the dynamics of the short EC VCSEL feedback system is an outcome of the interplay between delay-induced instabilities and PM competition. This becomes clear from the various complementary methods applied: the analysis of the time traces, the comparison of the power spectral densities, and the characteristics of the PDFs obtained from the time resolved cross-correlation analysis.

Additionally, in Fig. 14, we have included the cross-correlation coefficient at zero time lag also in the case of longer EC, namely 10 and 16 cm. Interestingly, at each EC length, the cross-correlation function behaves in a very similar way as in the case of shorter EC length, i.e., first increases at low current values and then gradually decreases, when passing the solitary laser threshold current. We mention that we have also investigated the low-frequency components of the PP dynamics at these longer EC lengths and we have checked that in the case of longer cavities the system also possesses correlation features similar to the ones depicted in Figs. 11 and 12. At these longer ECs, we observe a clear transition from the PP type II dynamics at low currents to the PP dynamics of type I at high current. All these low- and high-frequency features seem to be characteristic properties of the PM competition of VCSEL subject to delayed OF. This indicates the generality of the observed interplay between delay-induced dynamics and PM competition for the intensity dynamics of VCSELs with delayed OF. Furthermore, the strong interplay between both mechanisms can explain the identified differences between the dynamics of VCSELs and EELs with delayed OF. Consequently, our results also raise the question about the relevance of mode competition for PP dynamics for other types of lasers, e.g., for EELs with either a strong PM competition or longitudinal mode competition [39]. In particular, the question should be addressed, whether such lasers can exhibit similar dynamics originating from an interplay of delay-induced instabilities and either PM or longitudinal mode competition.

VI. CONCLUSIONS

In this paper, we have experimentally analyzed the intensity dynamics of a VCSEL with optical feedback in the short EC regime. We have demonstrated the existence of pulse package dynamics in the total intensity of the VCSEL feedback system. A detailed study of the spectral and autocorrelation properties of the PP dynamics in dependence on the injection current has revealed some similarities, but also distinct differences to the conventional dynamics reported in the case of short EC edge emitting lasers [18,23]. The major differences comprise the lack of qualitative changes of the dynamics for variations of the feedback phase, the significant variations of the amplitude of the fast intensity pulsations, and finally the distinct differences in the shape of the PP envelope. In order to gain insight into the origin of these differences, we have investigated the temporal behavior of the two polarization modes. We have identified two types of PP dynamics. On the PP envelope time scale, the dynamics can take place either in one of the two PM while the other mode is suppressed, defining type I PP dynamics, or the PP dynamics can occur in both PMs simultaneously, referred to as type II PP dynamics.

The spectral analysis has uncovered an anticorrelated behavior of the two PMs at frequencies lower than the PP envelope frequency, which reveals the continuous, much slower polarization mode hopping dynamics. Exactly at the PP envelope frequency and harmonics thereof, the dynamics is correlated or anticorrelated depending on the level of the injection current. Furthermore, we have analyzed the high-frequency dynamics of the fast intensity pulsations on the time scale of the EC round-trip frequency and we have provided evidence that correlation properties of the pulses can change from package to package or even within a single package, depending on the momentary difference between the PM intensities. We have found that the high-frequency pulses emitted at the delay in the two PM are correlated when the low-frequency PP dynamics is of type II. On the contrary, the pulses at the delay are anticorrelated if the slow dynamics is of type I. The progressive change of the dynamics with the injection current is connected also with an average phase shift between the emission of pulses in the two PMs, from 0, at low currents, to π, at high currents. Moreover, our cross-correlation analysis has shown that the appearance of the dynamics in one PM triggers the emission of pulses in the other PM. We have also compared the power spectral densities of the dynamics of the PMs with increasing the injection current and we have uncovered a gradual change from correlated to anticorrelated behavior for the high as well as for the low-frequency components of the PP dynamics. We have been able to quantify these changes of the correlation properties utilizing a time resolved correlation analysis. The application of a number of complementary techniques has identified the strong interplay of the delay-induced instabilities and the PM competition, as being the origin of the distinct differences between the total intensity short EC dynamics of VCSELs and EELs. This strong interplay of the two mechanisms, which we have revealed for PP dynamics of short EC VCSELs with weak intrinsic polarization anisotropy, seems to be of general nature. Therefore, similar mode competition effects might also be of relevance for the dynamics of other short EC systems, such as EELs systems with strongly coupled longitudinal modes.

ACKNOWLEDGMENTS

The authors acknowledge the support of the IAP Program of the Belgian government, as well as GOA, FWO, and OZR of the VUB and COST Action 288 "Nanoscale and ultrafast photonics." Furthermore, we thank S. Mandre for valuable support with the experiments and M. Antkowiak for technical help.

[1] C. Risch and C. Voumard, J. Appl. Phys. **48**, 2083 (1977).
[2] D. Lenstra, B. H. Verbeek, and A. J. den Boef, IEEE J. Quantum Electron. **QE-21**, 674 (1985).
[3] J. Mørk and B. Tromborg, IEEE Photonics Technol. Lett. **2**, 21 (1990).
[4] K. Peterman, IEEE J. Sel. Top. Quantum Electron. **1**, 480 (1995).
[5] C. Masoller and N. B. Abraham, Phys. Rev. A **57**, 1313 (1998).
[6] T. L. Paoli and J. E. Ripper, IEEE J. Quantum Electron. **QE-6**, 335 (1970).
[7] G. P. Agraval, IEEE J. Quantum Electron. **20**, 468 (1984).
[8] H. Olesen, J. H. Osmundsen, and B. Tromborg, IEEE J. Quantum Electron. **QE-22**, 762 (1986).
[9] T. Heil, I. Fischer, and W. Elsäßer, J. Opt. B: Quantum Semiclassical Opt. **2**, 413 (2000).
[10] C. R. Mirasso, P. Colet, and P. Garcia-Fernández, IEEE Photonics Technol. Lett. **8**, 299 (1996).
[11] V. Annovazzi-Lodi, S. Donati, and A. Scire, IEEE J. Quantum Electron. **QE-32**, 953 (1996).
[12] I. Fischer, Y. Liu, and P. Davis, Phys. Rev. A **62**, 011801(R) (2000).
[13] M. Peil, I. Fischer, and W. Elsäßer, C. R. Phys. **5**, 633 (2004).
[14] P. Ruprecht and J. Brandenberger, Opt. Commun. **93**, 82 (1992).
[15] F. Y. Lin and H. M. Liu, IEEE J. Sel. Top. Quantum Electron. **STQE-10**, 991 (2004).
[16] R. W. Tkach and A. R. Chraplyvy, J. Lightwave Technol. **LT-4**, 1655 (1986).
[17] Y. Ikuma and J. Ohtsubo, IEEE J. Quantum Electron. **34**, 1240 (1998).
[18] T. Heil, I. Fischer, W. Elsäßer, and A. Gavrielides, Phys. Rev. Lett. **87**, 243901 (2001).
[19] T. Sano, Phys. Rev. A **50**, 2719 (1994).
[20] G. V. Tartwijk, A. Levine, and D. Lenstra, IEEE J. Sel. Top. Quantum Electron. **1**, 466 (1995).
[21] A. Gavrielides, T. C. Newell, V. Kovanis, R. G. Harrison, N. Swanston, D. Yu, and W. Lu, Phys. Rev. A **60**, 1577 (1999).
[22] R. L. Davidchack, Y.-C. Lai, A. Gavrielides, and V. Kovanis, Phys. Rev. E **63**, 056206 (2001).
[23] T. Heil, I. Fischer, W. Elsäßer, B. Krauskopf, K. Green, and A. Gavrielides, Phys. Rev. E **67**, 066214 (2003).
[24] A. Tabaka, K. Panajotov, I. Veretennicoff, and M. Sciamanna, Phys. Rev. E **70**, 036211 (2004).
[25] Y. Chung and Y. Lee, IEEE Photonics Technol. Lett. **3**, 597 (1991).
[26] K. D. Choquette, R. Schneider, K. Lear, and R. Leibenguth, IEEE J. Sel. Top. Quantum Electron. **1**, 661 (1995).
[27] M. P. van Exter, M. B. Willemsen, and J. P. Woerdman, Phys. Rev. A **58**, 4191 (1998).
[28] B. Ryvkin, K. Panajotov, A. Georgievski, J. Danckaert, M. Peeters, G. Vershaffelt, H. Thienpont, and I. Veretennicoff, J. Opt. Soc. Am. B **16**, 2106 (1999).
[29] K. Panajotov, J. Danckaert, G. Verschaffelt, M. Peeters, B. Nagler, J. Albert, B. Ryvkin, H. Thienpont, and I. Veretennicoff, in *Polarization Behavior of Vertical-cavity Surface Emitting Lasers: Experiments, Models and Applications*, edited by M. Bertolotti, C. M. Bowden, and C. Sibilia, AIP Conf. Proc. No. 560 (AIP, Melville, New York, 2001).
[30] M. Giudici, S. Balle, T. Ackemann, S. Barland, and J. Tredicce, J. Opt. Soc. Am. B **16**, 2114 (1999).
[31] M. Sciamanna, K. Panajotov, H. Thienpont, I. Veretennicoff, P. Mégret, and M. Blondel, Opt. Lett. **28**, 1543 (2003).
[32] M. Sondermann, H. Bohnet, and T. Ackemann, Phys. Rev. A **67**, 021802(R) (2003).
[33] M. Sciamanna, A. Tabaka, H. Thienpont, and K. Panajotov, J. Opt. Soc. Am. B **22**, 777 (2005).
[34] M. Sciamanna, C. Masoller, N. B. Abraham, F. Rogister, P. Mégret, and M. Blondel, J. Opt. Soc. Am. B **20**, 37 (2003).
[35] A. V. Naumenko, N. A. Loiko, M. Sondermann, and T. Ackemann, Phys. Rev. A **68**, 033805 (2003).
[36] P. Mandel, B. A. Nguyen, and K. Otsuka, Quantum Semiclassic. Opt. **9**, 365 (1997).
[37] A. Uchida, Y. Liu, I. Fischer, P. Davis, and T. Aida, Phys. Rev. A **64**, 023801 (2001).
[38] M. Sondermann and T. Ackemann, Opt. Express **13**, 2707 (2005).
[39] G. Vaschenko, M. Giudici, J. J. Rocca, C. S. Menoni, J. R. Tredicce, and S. Balle, Phys. Rev. Lett. **81**, 5536 (1998).